# Weierstraß-Institut
## für Angewandte Analysis und Stochastik

im Forschungsverbund Berlin e.V.

Preprint ISSN 0946 – 8633


# A 1D coupled Schrödinger drift–diffusion model including collisions


Michael Baro[1], Naoufel Ben Abdallah[2],

Pierre Degond[2],Asma El Ayyadi[3]



submitted: 22nd April 2004



[1] Weierstrass Institute
for Applied Analysis and Stochastics
Mohrenstrasse 39
10117 Berlin, Germany
E-Mail: baro@wias-berlin.de

[2] MIP, UMR 5640 (CNRS-UPS-INSA)
Université Paul Sabatier
118, route de Narbonne
31062 Toulouse cedex, France
E-Mail: naoufel@mip.ups-tlse.fr
E-Mail: degond@mip.ups-tlse.fr

[3] Fachbereich Mathematik und Informatik
Johannes Gutenberg–Universität
Staudingerweg 9
55099 Mainz, Germany
E-Mail: elayyadi@mathematik.uni-mainz.de



No. 923
Berlin 2004

2000 *Mathematics Subject Classification.* 65Z05, 82D37, 78A35, 82C70, 34L40, 34L30, 34L25.

*Key words and phrases.* quantum–classical coupling, Schrödinger equation, scattering states, Pauli master equation, drift–diffusion, interface conditions.

Edited by
Weierstraß-Institut für Angewandte Analysis und Stochastik (WIAS)
Mohrenstraße 39
10117 Berlin
Germany

Fax: + 49 30 2044975
E-Mail: preprint@wias-berlin.de
World Wide Web: http://www.wias-berlin.de/

**Abstract**

We consider a one–dimensional coupled stationary Schrödinger drift–diffusion model for quantum semiconductor device simulations. The device domain is decomposed into a part with large quantum effects (quantum zone) and a part where quantum effects are negligible (classical zone). We give boundary conditions at the classic–quantum interface which are current preserving. Collisions within the quantum zone are introduced via a Pauli master equation. To illustrate the validity we apply the model to three resonant tunneling diodes.

# Contents

**1 Introduction** **2**

**2 Presentation of the Method** **3**
2.1 The quantum region . . . . . 3
2.2 The classical region . . . . . 4
2.3 The hybrid model . . . . . 5
2.3.1 Ballistic quantum zone . . . . . 6
2.3.2 Collisional quantum zone . . . . . 7

**3 Three test devices** **10**
3.1 The RTD of Mounaix *et al* [15] . . . . . 10
3.2 The RTD of Kluksdahl *et al* [14] . . . . . 18
3.3 The RTD of Fischetti [8] . . . . . 22

**4 Summary and Conclusion** **25**

# 1 Introduction

Quantum effects play an important role in nowadays semiconductor devices. The ongoing progress of industrial semiconductor device technologies permits to fabricate devices which inherently employ quantum phenomena in their operation, e.g. resonant tunneling diodes, quantum well laser, etc. The widely used drift–diffusion equation introduced by van Roosbroeck in 1950 [17], is not capable of properly taking into account these quantum effects. A finer level of modeling has to be used which is achieved by Schrödinger's or equivalently Wigner's equation. However the numerical treatment of these models is very expensive compared to the drift–diffusion model. In many semiconductor devices quantum effects take place in a localized region, e.g. around the double barrier in resonant tunneling diodes, whereas the rest of the device is well described by classical models like the drift–diffusion model. Thus it makes sense to follow a hybrid strategy: use a quantum model in regions where quantum effects are strong and couple this model by proper interface conditions to a classical model in the rest of the device domain.

In this paper we focus on a hybrid model, more precisely a coupled Schrödinger drift–diffusion model, which describes the transport in a resonant tunneling diode. Resonant tunneling diodes are typical examples for semiconductor devices whose functionality depends on quantum effects: Only particles with energies close to the resonant energy can pass through the double barrier. By tuning the applied bias one alters the resonant energy. The maximum current is achieved, if the Fermi energy in the source is equal to the resonant energy. If the resonant energy is below the Fermi energy of the source, the current decreases. This leads to the well known negative differential resistant effect observed in resonant tunneling diodes, i.e. in a certain region the current is decreasing with increasing voltage, see [19]. This non monotone current–voltage characteristics makes the resonant tunneling diodes very interesting in logic applications, as frequency filter, etc. The double barriers are in general sandwiched by highly doped regions in which a classical model would reasonable describe the electron transport. Therefore a hybrid model seems to be a useful strategy for resonant tunneling devices. The aim of this paper is to develop such a hybrid model in a one–dimensional stationary framework, by using a drift–diffusion model in the highly doped regions and Schrödinger's equation around the double barrier. The two models have to be coupled such that the continuity of the classical and quantum current is preserved, which is a physical consistent condition for the coupling. To take into account many particle effects, a self–consistent resolution of the coupled model with Poisson's equation is required.

In [3] a coupled kinetic–quantum model has been introduced, where the Schrödinger equation was used to define the density in the quantum zone. A Boltzmann equation in the classical zones is used to describe the density in the rest of the device domain. At the classical–quantum interface reflection–transmission conditions, i.e. boundary conditions for the Boltzmann equation depending on the reflection and transmission coefficient, have been defined. The distribution function which solves the Boltzmann equation with these reflection–transmission conditions was then used as "alimentation function" to construct the density in the quantum zone. Poisson's equation was used for a self–consistent resolution of the electrostatic potential. It was shown that the reflection–transmission conditions are current preserving. The quantum region was treated as ballistic, whereas the the classical regions can be highly collisional by choosing a proper collision operator in the Boltzmann equation.

Another hybrid model, which is more closely related to the model we will treat in this paper, was introduced in [6] and [7]. The Boltzmann equation together with the reflection–transmission conditions of the kinetic–quantum model of [3] was replaced by the drift–diffusion equation and corresponding connection conditions by the use of a diffusion approximation. The treatment of the quantum region and the Poisson equation is left as in [3]. Since the connection conditions is obtained by a boundary layer analysis of the reflection–transmission conditions, there exists only approximate formulas of the connection conditions for the drift–diffusion equation. Here we aim at a direct coupling of drift–diffusion and quantum models. Therefore, we will get analytic expression for the connection conditions.

The two hybrid models described above, i.e. [3] and [6], assume that the quantum region is ballistic and collisions are only taken into account in the classical regions. But electron–phonon collisions play an important role also in the quantum region. One possibility to model collisions is to use the Wigner formalism in the quantum zone with a semiclassical collision operator. Due to the possible non–positivity

of the Wigner distribution function, this approach is doubtful. Here we use a Pauli master equation approach to model collisions in the quantum zone, i.e. the distribution function in the quantum region is determined by a master equation which consists of a Pauli operator (modeling the collisions) and an interaction term with the classical regions.

The paper is organized as follows. In section 2 we present the coupled Schrödinger drift–diffusion equation, where we consider first the case where the quantum zone is treated ballistically and then the case where collisions are included by a Pauli master equation approach. In section 3 the hybrid models are validated against three resonant tunneling diode test cases to illustrate the validity of the models. We close with conclusions in section 4

# 2 Presentation of the Method

In this section we will present the strategy to couple Schrödinger and drift–diffusion equation. We assume that the device domain $\Lambda = (0, L)$ is divided into a quantum zone $\mho = (x_1, x_2)$ and a classical region $\Omega = \Lambda \setminus \mho$, where $0 < x_1 < x_2 < L$. In order to define the density and current of the coupled Schrödinger drift–diffusion model, we will first assume that the electrostatic potential $W$ is given on $\Lambda$ and later pose the Poisson equation which $W$ has to solve. Let $\Delta E$ denote the band–edge offset, for simplicity we define $V = W + \Delta E$.

## 2.1 The quantum region

We consider the potential $\widetilde{V}$ defined by

$$\widetilde{V}(x) = \begin{cases} V_1 := V(x_1), & \text{for } x \le x_1, \\ V(x), & \text{for } x \in \mho, \\ V_2 := V(x_2), & \text{for } x \ge x_2, \end{cases}$$

i.e. the potential $\widetilde{V}$ coincides with the potential $V$ inside the quantum zone $\mho$ and is extended continuously to the whole real line. To fix our ideas we assume that $V_2 > V_1$ and set $\delta V := V_2 - V_1$. Furthermore, we assume that the effective mass $m = m(x)$, $x \in \mathbb{R}$, is strictly positive and is constant outside the quantum zone $\mho$ with the same value, which we denote by $m$.

We consider the Schrödinger equation

$$\left( -\frac{\hbar^2}{2} \frac{d}{dx} \frac{1}{m(x)} \frac{d}{dx} - e\widetilde{V}(x) \right) \psi_p(x) = E_p \psi_p(x), \qquad x \in \mathbb{R}, \qquad p \in \mathbb{R}, \tag{1}$$

where

$$E_p = \begin{cases} \frac{p^2}{2m} - eV_1, & p > 0 \\ \frac{p^2}{2m} - eV_2, & p < 0, \end{cases}$$

$e$ denotes the elementary charge (positive) and $\hbar$ is the scaled Planck constant. The operator (1) has been intensively studied, see e.g. [5, 4, 1, 11, 10]. For $p > 0$, $\psi_p$ denote the right–going scattering states, whereas $\psi_p$, $p < 0$, denote the left–going scattering states. In the regions $x < x_1$ and $x > x_2$ the solutions of Schrödinger's equation are given by a superposition of plane waves, i.e.

$$\psi_p(x) = \begin{cases} \exp\left(i\frac{p}{\hbar}(x - x_1)\right) + r(p) \exp\left(-i\frac{p}{\hbar}(x - x_1)\right), & x < x_1, \\ t(p) \exp\left(i\frac{p_+}{\hbar}(x - x_2)\right), & x > x_2, \end{cases} \quad \text{for } p > 0, \tag{2a}$$

and

$$\psi_p(x) = \begin{cases} t(p) \exp\left(-i\frac{p_-}{\hbar}(x - x_1)\right), & x < x_1, \\ \exp\left(i\frac{p}{\hbar}(x - x_2)\right) + r(p) \exp\left(-i\frac{p}{\hbar}(x - x_2)\right), & x > x_2, \end{cases} \quad \text{for } p < 0, \tag{2b}$$

with

$$p_+ := \sqrt{p^2 + p_\delta^2}, \quad \text{and} \quad p_- := \sqrt{p^2 - p_\delta^2},$$

where $p_\delta = \sqrt{2em\delta V}$. The coefficients $t(p)$ and $r(p)$ denote the transmission and reflection amplitudes, respectively. The transmission and reflection coefficients are then defined by

$$T(p) = \begin{cases} \frac{p_+|t(p)|^2}{|p|}, & p > 0 \\ \frac{p_-|t(p)|^2}{|p|}, & p < 0, \end{cases} \qquad \text{and} \quad R(p) = |r(p)|^2.$$

We have the following relations between the transmission and reflection coefficient

$$T(p) + R(p) = 1, \qquad \text{for all } p \in \mathbb{R},$$

$$\begin{aligned} &T(p) = T(-p_+), \text{ for all } p > 0, \quad T(p) = T(p_-), \text{ for all } p < -p_\delta, \\ &R(p) = 1, \text{ for } -p_\delta < p < 0. \end{aligned} \tag{3}$$

Using the asymptotics (2) of the scattering states $\psi_p$, one can derive boundary conditions for $\psi_p$ at the boundaries $x_1$ and $x_2$, see [6, 7, 10, 1]. Furthermore, note that the transmission and reflection amplitudes are given in terms of $\psi_p(x_i)$ and $\psi_p'(x_i)$, $i = 1, 2$, see [6, 1] for details. This allows a numerical treatment of the Schrödinger equation.

Let $g(p)$, $p \in \mathbb{R}$, be a given distribution function. The quantum density in the region $\mathfrak{V}$ is given by

$$n_Q(x) := \int_{\mathbb{R}} g(p)|\psi_p(x)|^2 dp, \qquad x \in \mathfrak{V}. \tag{4}$$

The current is defined by

$$j_Q(x) := \int_{\mathbb{R}} g(p)\mathfrak{Im}\left(\frac{\hbar}{m(x)}\frac{\partial}{\partial x}\psi_p(x)\overline{\psi_p(x)}\right) dp, \qquad x \in \mathfrak{V}. \tag{5}$$

It is not difficult to see that the current density does not depend on $x$. Furthermore, a straightforward computation, using asymptotics of $\psi_p$, i.e. (2), and the relations (3), gives the following expression for $j_Q$

$$j_Q = \int_0^\infty v_p T(p)\left(g(p) - g(-p_+)\right) dp, \tag{6}$$

where $v_p$ is the electron group velocity given by $v_p := \frac{d}{dp}E_p = \frac{p}{m}$.

## 2.2 The classical region

We consider a stationary drift–diffusion model on the disconnected domain $\Omega$, i.e.

$$\begin{aligned} -\frac{d}{dx}j_C &= 0, \\ j_C &= \mu n_C \frac{d}{dx}\varphi, \\ n_C &= F(V - \varphi), \end{aligned} \tag{7}$$

where $\mu \in \mathbb{R}$, $\mu > 0$, is the mobility of electrons, $F$ describes the dependence of the carrier density $n_C$ on the chemical potential and $\varphi$ is the unknown electro–chemical potential. We assume that $F$ is either

$$F(s) = N_0 \exp(s/U_{th}) \qquad \text{Boltzmann statistic}, \tag{8}$$

or

$$F(s) = N_0 \frac{2}{\sqrt{\pi}} \int_0^\infty \frac{\sqrt{t}\, dt}{1 + \exp(t - s/U_{th})} \qquad \text{Fermi–Dirac statistic,} \tag{9}$$

where $U_{th} = k_B T/e$ denotes the thermal potential ($k_B$ is the Boltzmann constant and $T$ the lattice temperature) and $N_0 = 2\left(\frac{k_B T m}{2\pi\hbar^2}\right)^{3/2}$ is the effective density of states. We impose the following boundary conditions

$$\varphi(0) = \varphi_0, \qquad \varphi(L) = \varphi_L, \tag{10}$$

$$j_C(x_1) = j_C(x_2) = h(\varphi(x_1)) - h(\varphi(x_2)), \tag{11}$$

where $\varphi_0, \varphi_L \in \mathbb{R}$ are given and $h$ is a real–valued and monotonously decreasing function which will be determined later by the quantum mechanical expression for the current.

The system (7) with the boundary conditions (10) has a unique (weak) solution $\varphi$. This can be seen by writing

$$\int_\Omega A(\varphi)\psi dx = \int_\Omega \mu F(V-\varphi)\frac{d}{dx}\varphi\frac{d}{dx}\psi dx + \left[h(\varphi(x_1)) - h(\varphi(x_2))\right]\left[\psi(x_2) - \psi(x_1)\right], \tag{12}$$

for all $\varphi \in W^{1,2}(\Omega)$, $\psi \in \{\psi \in W^{1,2}(\Omega) \,|\, \psi(0) = \psi(L) = 0\}$. Using the Lax–Milgram theorem, see[12], one can show that there exists a weak solution of the drift–diffusion model. We refer to [2] for the details.

Let us now consider the special case where $F$ is given by (8) and $h$ of the form

$$h(\xi) = \Theta^{-1}\exp(-\xi/U_{th}), \qquad \Theta > 0. \tag{13}$$

The boundary condition (10) can then be written as

$$\varphi(0) = \varphi_0, \qquad \varphi(L) = \varphi_L, \tag{14}$$

$$j_C(x_1) = j_C(x_2) =: j_C, \tag{15}$$

$$\exp(-\varphi(x_1)/U_{th}) - \exp(-\varphi(x_2)/U_{th}) = \Theta j_C, \tag{16}$$

which are exactly the boundary conditions treated in [6]. Furthermore, one easily verifies that $\varphi$ is given by

$$\varphi(x) = \begin{cases} -U_{th}\ln\left[\exp\left(-\varphi_0/U_{th}\right) - j_C/(U_{th}\mu N_0)\int_0^x \exp\left(-V(t)/U_{th}\right)dt\right], & x \in (0, x_1), \\ -U_{th}\ln\left[\exp\left(-\varphi_L/U_{th}\right) + j_C/(U_{th}\mu N_0)\int_x^L \exp\left(-V(t)/U_{th}\right)dt\right], & x \in (x_2, L), \end{cases}$$

where

$$j_C = \frac{\exp\left(-\varphi_0/U_{th}\right) - \exp\left(-\varphi_L/U_{th}\right)}{\Theta + 1/(U_{th}\mu N_0)\int_\Omega \exp\left(-V(t)/U_{th}\right)dt}.$$

Clearly we have

$$j_C \gtreqless 0, \quad \text{iff} \quad \varphi_0 \gtreqless \varphi_L, \tag{17}$$

i.e. the direction of the current depends on the difference of the electro–chemical potential at the boundaries. Furthermore, we have in thermodynamic equilibrium, i.e. $\varphi_0 = \varphi_L = \phi$, that $\varphi(x) = \phi$, for all $x \in \Omega$, and $j_C = 0$.

## 2.3 The hybrid model

In this subsection we couple the quantum and the classical model considered in subsections 2.1 and 2.2. The two systems are coupled in such a way that the continuity of the classical and the quantum mechanical current over the whole device domain $\Lambda$ is guaranteed, i.e. $j_C = j_Q$.

We introduce the density of the hybrid model $n$ defined by

$$n(x) := \begin{cases} n_Q(x), & \text{for } x \in \mho \\ n_C(x), & \text{for } x \in \Omega. \end{cases} \tag{18}$$

Furthermore, the electrostatic potential has to satisfy Poisson's equation on the whole device domain $\Lambda$

$$-\frac{d}{dx}\epsilon\frac{d}{dx}W = e\,(n_D - n)\,, \tag{19a}$$

with Dirichlet boundary conditions

$$W(0) = 0, \qquad W(L) = W_L, \tag{19b}$$

where $n_D$ denotes the doping profile.

We will consider two different cases: (i) the quantum zone is treated ballistically, and (ii) collision in the quantum zone are introduced via a Pauli master equation.

### 2.3.1 Ballistic quantum zone

Let us first assume that the electro–chemical potential $\varphi$ at the interface is known. We define the distribution function $g$ by

$$g(p) := \begin{cases} f(E_p + e\varphi(x_1)), & \text{for } p > 0 \\ f(E_p + e\varphi(x_2)), & \text{for } p < 0, \end{cases} \tag{20}$$

where $f$ is the distribution function of reduced carrier gas, i.e.

$$f(s) = n_0 \exp\left(-s/(k_B T)\right), \qquad \text{Boltzmann statistic,} \tag{21}$$

or

$$f(s) = n_0 \ln\left(1 + \exp(-s/(k_B T))\right), \qquad \text{Fermi–Dirac statistic,} \tag{22}$$

with $n_0 = (m k_B T)/(2\pi^2\hbar^3)$. Inserting this in the expression (6) for the quantum current we obtain

$$j_Q = h(\varphi(x_1)) - h(\varphi(x_2)),$$

with

$$h(\xi) = \int_0^\infty v_p T(p) f(E_p + e\xi) dp, \tag{23}$$

since $E_p = E_{-p_+}$, for all $p > 0$. Clearly $h$ is monotonously decreasing, since $f$ is monotonous. Using the function $h$ defined by (23) in the boundary conditions of the drift–diffusion equation (10) guarantees the continuity of the classical and quantum current, i.e. $j_Q = j_C$.

Therefore we look for a fixed point of the following mapping: Assume that $W$ is a first guess of the electrostatic potential. Solving the Schrödinger equation (1) we obtain the scattering functions $\psi_p$ and the transmission coefficient $T(p)$. Thus we can compute the function $h$ by (23). Solving the drift–diffusion equation (7) with boundary conditions (10), we obtain the electro–chemical potential $\varphi$ and consequently the classical density $n_C$. The quantum density is then determined by (4) with $g$ given by (20). Solving Poisson's equation (19) we obtain a new potential $W_{new}$.

In the special case where $f$ is given by the Boltzmann distribution (21), we get for the function $h$

$$h(\xi) = \Theta^{-1} \exp\left(-\xi/U_{th}\right),$$

with

$$\Theta^{-1} = n_0 \int_0^\infty v_p T(p) \exp\left(-E_p/(k_B T)\right) dp, \tag{24}$$

see (13). The positivity of $\Theta$ is obvious.

The coupling of the drift–diffusion and Schrödinger equations described above is closely related to the coupling used in [6], see also [7]. In [6] a diffusion approximation of the kinetic–quantum model introduced in [3] was used which led to boundary conditions of the form (14)–(16). The constant $\Theta$ was obtained by the approximation of the reflection–transmission conditions of [3] at the interface. There exists no analytic formula of the coupling constant $\Theta$ used in [6], but several different approximate expressions for $\Theta$. A closer look at this approximated formulas shows, that the $\Theta$ given by (24) is the leading term. The reflection–transmission of the kinetic–quantum model [3] ensures the continuity of the kinetic and quantum current at the interface. Looking at the diffusion approximation used in [6] we see that the continuity of the drift–diffusion and quantum current is only preserved up to order $\alpha$, where $\alpha$ is the small parameter of the diffusion approximation. By our choice of $\Theta$ we obtain an exact continuity of the current and an analytic expression for the constant $\Theta$.

### 2.3.2 Collisional quantum zone

To introduce collisions, not only in the classical zone, but also in the quantum zone, we use a Pauli master equation approach [16]. The distribution function $g$ is determined by an equation of the form

$$\partial_t g = Pg + Cg, \tag{25}$$

where $P$ is the so–called Pauli operator (modeling the collision effects) and $C$ is a operator modeling the interaction with classical regions. The operator $C$ is of the form

$$Cg = (\partial_t g)^+ - (\partial_t g)^- ,$$

where the terms $(\partial_t g)^\pm$ are gain and loss terms, respectively. The Pauli operator $P$ is in general of the form

$$(Pg)(p) = \int_{\mathbb{R}} W_{p'\to p} g(p') d\rho(p') - \int_{\mathbb{R}} W_{p\to p'} g(p) d\rho(p').$$

$W_{p\to p'}$ is the rate of transition from state $p$ to $p'$ and the measure $d\rho(p)$, i.e. the density of states, is given by

$$d\rho(p) = \left( \int_{x_1}^{x_2} |\psi_p(x)|^2 dx \right) dp.$$

We make the following hypothesis for the transition rate $W_{p\to p'}$: There exists a symmetric function $\Phi_{pp'}$ such that

$$W_{p\to p'} = \Phi_{pp'} f_0(p'), \qquad f_0(p) := \frac{f(E_p)}{\mathcal{N}_{eq}},$$

where $f$ is either given by the Boltzmann or the Fermi–Dirac distribution function, i.e. (21) or (22) and $\mathcal{N}_{eq}$ is the total number of particles in the quantum zone with respect to the equilibrium distribution function, i.e.

$$\mathcal{N}_{eq} = \int_{\mathbb{R}} f(E_p) d\rho(p).$$

$f_0$ is called the (normalized) quantum mechanical equilibrium distribution function and $\Phi_{pp'}$ the collision cross section. We note that $\int_{\mathbb{R}} f_0(p) d\rho(p) = 1$.

To simplify our considerations, we make a relaxation time approximation, i.e. we assume that $\Phi_{pp'}$ is independent of $p$ and $p'$ and given by $\Phi_{pp'} = 1/\tau_Q$, where $\tau_Q$ is the relaxation time. Therefore, the Pauli operator is the linear operator given by

$$(Pg)(p) = \frac{1}{\tau_Q} \left( f_0(p) \int_{\mathbb{R}} g(p') d\rho(p') - g(p) \int_{\mathbb{R}} f_0(p) d\rho(p) \right). \tag{26}$$

The source terms $(\partial_t g)^\pm$ model the interaction of the classical and quantum mechanical regions. To evaluate these terms we assume for the moment that the electro–chemical potential $\varphi$ at the interface

boundaries $x_1$ and $x_2$ is known. Assuming that the particle that enter the quantum zone at $x_1$ and $x_2$ with momentum $p$ are distributed by $f(E_p + e\varphi(x_1))$, $p > 0$, respectively $f(E_p + e\varphi(x_2))$, $p < 0$, where $f$ is given by (21) or (22), we get for the gain term

$$(\partial_t g)^+ (p) = \nu_p f_1(p),$$

with

$$f_1(p) = \begin{cases} f(E_p + e\varphi(x_1)), & \text{for } p > 0, \\ f(E_p + e\varphi(x_2)), & \text{for } p < 0. \end{cases}$$

The loss term $(\partial_t g)^-$ is given by

$$(\partial_t g)^- (p) = \nu_p g(p), \qquad p \in \mathbb{R},$$

where $\nu_p$ is a gain or loss rate of particle through the interface given by

$$\nu_p := \frac{|v_p|}{\int_{x_1}^{x_2} |\psi_p(x)|^2 dx}.$$

The term $\int_{x_1}^{x_2} |\psi_p(x)|^2 dx$ can be interpreted as the size of the quantum region for particles of momentum $p$. Note that $\psi_p$ will be almost a free wave for momenta $p$ corresponding to energies much larger than the maximal potential energy. Thus $\nu_p \approx |v_p|/(x_2 - x_1)$ for $p$ with $E_p \gg \max_{x\in\mho}\{-eV(x)\}$. For momenta $p$ with energies $E_p$ equal to resonant energies, the wave function $\psi_p$ will be very localized in the quantum region and consequently the value of $\int_{x_1}^{x_2} |\psi_p(x)|^2 dx$ will be very large. Hence, $\nu_p \approx 0$ for such $p$. Thus the factor $\nu_p$ takes into account that the resonant states cannot be fed as strong as the other states by the classical regions. The resonant states are fed by the scattering mechanism introduced by the Pauli operator $P$. The probability that a carrier in any state $p$ will be scattered into the momentum volume $dp'$ is given by $W_{p\to p'} d\rho(p')$, which is by our assumption equal to

$$\frac{f(E_{p'})}{\tau_Q \mathcal{N}_{eq}} \left( \int_{x_1}^{x_2} |\psi_{p'}(x)|^2 dx \right) dp'. \tag{27}$$

This probability will be very large for $p'$ corresponding to energies equal to a resonant energy, which shows that the resonant states are fed by the collision mechanism.

The stationary Pauli master equation, i.e. $\partial_t g = 0$ in (25), can be written as

$$\nu_p g(p) - (Pg)(p) = \nu_p f_1(p)$$

Inserting the expression (26) in the above equation we obtain

$$\left(\nu_p + \frac{1}{\tau_Q}\right) g(p) - \frac{1}{\tau_Q} f_0(p) \int_{\mathbb{R}} g(p') d\rho(p') = \nu_p f_1(p) \tag{28}$$

After some computation we find

$$g(p) = \kappa_p A f(E_p) + (1 - \kappa_p) f_1(p), \tag{29}$$

with

$$\kappa_p := \frac{1}{1 + \tau_Q \nu_p} \quad \text{and} \quad A := \frac{\int_{\mathbb{R}} (1 - \kappa_{p'}) f_1(p') d\rho(p')}{\int_{\mathbb{R}} (1 - \kappa_{p'}) f(E_{p'}) d\rho(p')}. \tag{30}$$

We remark that $0 < \kappa_p < 1$, for all $p \in \mathbb{R}$. Furthermore, the total number of particle in the quantum region $\mathcal{N}$ is given by

$$\mathcal{N} = \int_{\mathbb{R}} g(p) d\rho(p) = A\mathcal{N}_{eq}.$$

Therefore, $A$ can be written as

$$A = \frac{\mathcal{N}}{\mathcal{N}_{eq}}, \tag{31}$$

i.e. $A$ is the ratio of the total number of particles $\mathcal{N}$ and the number of particles with respect to the equilibrium distribution $\mathcal{N}_{eq}$.

If the relaxation time $\tau_Q$ tends to infinity (zero), we get that $\kappa_p$ tends to zero (one). Thus we get from the expression (29)

$$\lim_{\tau_Q \to \infty} g(p) = f_1(p), \tag{32}$$

and

$$\lim_{\tau_Q \to 0} g(p) = A_\infty f(E_p), \quad \text{where} \quad A_\infty = \lim_{\tau_Q \to 0} A = \frac{\int_{\mathbb{R}} \nu_p f_1(p) d\rho(p)}{\int_{\mathbb{R}} \nu_p f(E_p) d\rho(p)}. \tag{33}$$

Since $f_1$ is equal to the distribution function in the ballistically case, see subsection 2.3.1 equation (20), we get that for an infinite relaxation time the collisional hybrid model is equal to the ballistically hybrid model of subsection 2.3.1. Furthermore, for $\tau_Q \to 0$ we obtain—as aspected—$g(p) = A_\infty f(E_p)$, i.e. we end up in an equilibrium situation.

To simplify our considerations in the following, we will assume that $f$ is given by the Boltzmann distribution function (21). A straightforward computation gives

$$A := \sigma \exp(-\varphi(x_1)/U_{th}) + (1-\sigma)\exp(-\varphi(x_2)/U_{th}),$$

with

$$\sigma := \frac{\int_0^\infty (1-\kappa_p) f(E_p) d\rho(p)}{\int_{\mathbb{R}} (1-\kappa_p) f(E_p) d\rho(p)}.$$

Inserting the expression (29) in equation (6) we get

$$j_Q = h(\varphi(x_1)) - h(\varphi(x_2)), \tag{34}$$

with

$$h(\xi) = \Theta^{-1} \exp(-\xi/U_{th}), \tag{35}$$

where

$$\Theta^{-1} = n_0 \int_0^\infty v_p T(p) \exp(-E_p/(k_B T)) \left(1 - (1-\sigma)\kappa_p - \sigma\kappa_{-p_+}\right) dp. \tag{36}$$

Note that in equilibrium, i.e. $\varphi_1 = \varphi_2 = \phi$, we have $g(p) = f(E_p + e\phi)$. Hence there are no collision events in equilibrium. Furthermore, the current vanishes in equilibrium.

We use the function $h$ defined in (35) in the boundary conditions of the drift–diffusion equation (7) and therefore guarantee the continuity of the current, if the distribution function $g$ is a solution of the Pauli master equation (28). The positivity of $\Theta$ follows immediately from the fact that $0 < \kappa_p < 1$ for all $p \in \mathbb{R}$.

Thus we look for a solution of the following mapping: Assume that $W$ is given. Calculating the transmission coefficient $T(p)$, we obtain the constant $\Theta$ by (36). Solving the drift–diffusion equations (7) we obtain the classical density $n_C$, solve the Pauli master equation to obtain the distribution function $g$, see (29), and obtain the quantum density $n_Q$. Solving Poisson's equation with $n$ given by (18) we get a new potential $W_{new}$.

Since $\kappa_p \to 0$ if $\tau_Q \to \infty$, we get by (24) and (36) that $\Theta_{col} \to \Theta_{bal}$ if $\tau_Q \to \infty$, where $\Theta_{bal}$ is given by (24) and $\Theta_{col}$ by (36). Thus if the relaxation time $\tau_Q$ tends to infinity, we obtain—as aspected—the ballistic hybrid model of subsection 2.3.1.

In the case where the distribution function $f$ is given by the Fermi–Dirac function (22) we cannot write $j_Q$ in the form (34) and thus the techniques used here to couple the drift–diffusion and Schrödinger equation do not apply so straightforwardly.

# 3 Three test devices

In this section we apply the coupling methods presented in the previous section to three resonant tunneling diodes dealt with in the literature. The first one was treated by Mounaix *et al* [15], the second by Kluksdahl *et al* [14], and the third one by Fischetti [8].

We use the Boltzmann statistics in the classical and quantum zone, i.e. $F$ is given by (8) and $f$ by (21). As boundary conditions for the drift–diffusion equation we assume

$$n_C(0) = N_D, \qquad n_C(L) = N_D,$$

where $N_D = n_D(0) = n_D(L)$ ($n_D$ denotes the doping profile). The Poisson equation is treated with the boundary conditions given in (19). Furthermore, the band–edge offset $\Delta E$ is equal to zero in the classical zone. Therefore, $W(x) = V(x)$ for all $x \in \Omega$. The mobility is given by $\mu = \tau_C e/m$, where $\tau_C$ is the mean collision time in the classical zone. The density in the classical zone is then given by

$$n_C(x) = \begin{cases} N_D \exp\left(W(x)/U_{th}\right) - j/(U_{th}\mu) \int_0^x \exp\left((W(x) - W(t))/U_{th}\right) dt, & x \in (0, x_1) \\ N_D \exp\left((W(x) - W_L)/U_{th}\right) + j/(U_{th}\mu) \int_x^L \exp\left((W(x) - W(t))/U_{th}\right) dt, & x \in (x_2, L), \end{cases}$$

where

$$j = \frac{\left[1 - \exp(-W_L/U_{th})\right](N_D/N_0)}{\Theta + 1/(U_{th}\mu N_0) \int_\Omega \exp(-W(t)/U_{th}) dt}.$$

The constant $\Theta$ depends on the quantum zone and is given by (24), if the quantum zone is treated ballistically, and by (36), if collisions are included in the quantum zone. To distinguish between the two different $\Theta$'s we will write $\Theta_{bal}$ for (24) and $\Theta_{col}$ for (36). Schrödinger's equation is discretized as described in [6] and Poisson's equation in solved by the Gummel method, see e.g. [18].

## 3.1 The RTD of Mounaix *et al* [15]

The first device we consider is the resonant tunneling diode investigated by Mounaix *et al* in [15]. The geometry of the device is depicted in Figure 1. It consists of 5 nm tunnel barriers of $Al_{0.3}Ga_{0.7}As$ separated by a 5 nm GaAs undoped well. The double–barrier heterostructure is placed between two undoped 2.5 nm claddings and two 50 nm GaAS spacer layer with a doping density of $2 \cdot 10^{16}\text{cm}^{-3}$. These spacer are enclosed by two $2 \cdot 10^{18}\text{cm}^{-3}$ GaAs doped cap layer of 500 nm width. This leads to a total device length of $L = 1120$ nm.

The double barrier height $H$ is of 0.23 eV and the relative permittivity $\epsilon$ is constant over the whole device with $\epsilon = 12.4\epsilon_0$. The effective mass is $m_1 = 0.067\, m_0$ in the GaAs regions and $m_2 = 0.092\, m_0$ in the barriers. The temperature is fixed at room temperature $T = 300$ K. The physical values are summarized in Table I.

| $m_1$ | $m_2$ | $\epsilon$ | $T$ [K] | $H$ [eV] |
|---|---|---|---|---|
| $0.067m_0$ | $0.092m_0$ | $12.4\epsilon_0$ | 300 | 0.23 |

Table I: Physical parameters for the device of [15], where the index 1 refers to the GaAs regions and 2 to the barrier region

The current–voltage characteristics obtain in the ballistic and collision case is displayed in Figure 2. The quantum zone was places at the $N^+$–$N$ and $N$–$N^+$ junctions, i.e. $x_1 = 500$ nm and $x_2 = 620$ nm. $\tau_C$ is chosen to be $3.24 \cdot 10^{-13}$s and in the collision case we set $\tau_Q$ equal to $\tau_C$, i.e. $\tau_C = \tau_Q = \tau$.

Our results differ in several ways with those of [15]. First in [15] two current peaks are observed, a flat one around 0.26 V and a sharp one at 0.32 V. We find only one current peak at 0.25 V. Furthermore, our values of the peak current density are a factor two below that of [15]. This is probably due to the collisionless treatment of the device in [15].

A comparison with the method used on [6] and the ballistic coupling introduced in section 2.3.1, shows that the current–voltage characteristic obtained by our model coincides with that obtained in [6] by the

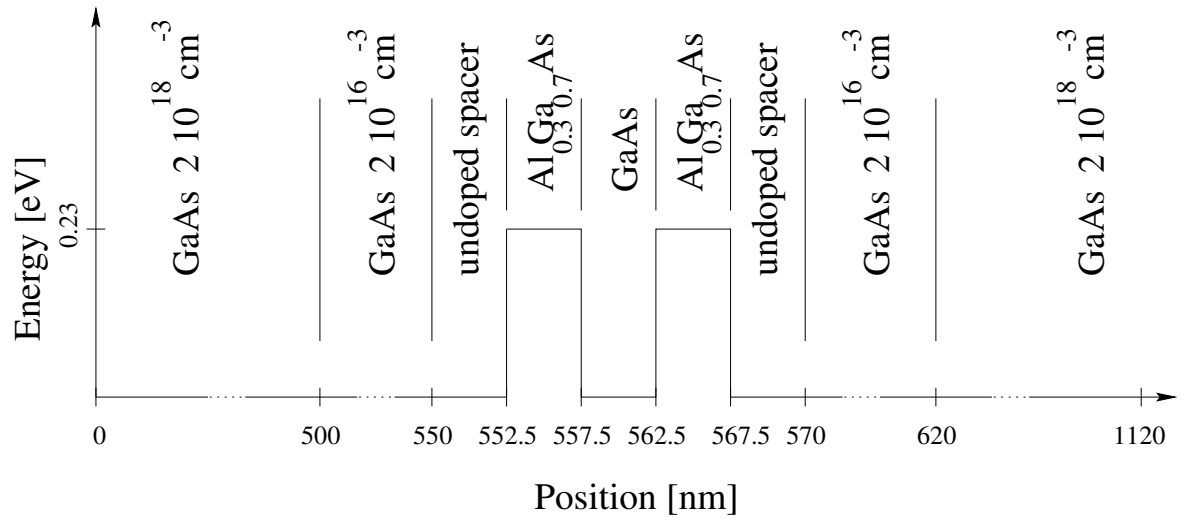


Figure 1: The double barrier resonant tunneling structure of [15]

Marshak approximation of the coupling constant $\Theta$. This is not surprising, since the coupling constant defined by (24) is the dominant factor in the Marshak coupling constant used in [6].

Looking at the ballistic and the collision current–voltage characteristics plotted in Figure 2 we see that the collisionless current is larger than the collision current for an applied voltage up to 0.25 V. The potential profiles for a series of applied biases are shown in Figure 3. We observe that the potential bump on the left hand side of the double barrier only changes significantly in the ballistically case, if the applied bias passes the current peak bias. In the collisional case this potential bump is monotonically lowered with increasing bias. This is explained by the probability (27): We see from equation (27) that particles entering the quantum zone at $x_1$ with momentum $p > 0$ have very high probability to be scattered to states with energy $E_{p'} \approx -eV_2$, i.e. to change there momentum to $p' < 0$. Hence particles are transported from the left side to the right side of the double barrier due to the collision mechanism. Furthermore this effect is reflected in Figures 3 and 4 by noting that the "collisional potential/density" is smaller than the "ballistically potential/density" on the left hand side of the double barrier, whereas the opposite holds on the right hand side of the double barrier. The transmission coefficients corresponding to the current peak voltage are plotted in Figure 5. The first transmission resonance appears at $\epsilon_{bal} = 0.088\,\text{eV}$ in the ballistic case and $\epsilon_{col} = 0.055\,\text{eV}$ in the collision case. The distribution function in the ballistic and the collisional cases are shown in Figure 6. First we observe that $g_{col}(p) \leq g_{bal}(p)$ for $p > 0$ and $g_{col}(p) \geq g_{bal}(p)$ for $p < 0$, which also reflects the transport of particles from the left side to the right side of the barrier due to collisions. In the collisional case we observe that $g(p)$ is almost zero for $p$ corresponding to the resonance energies. This can be seen from the formula (29): As already mentioned in subsection 2.3.2 $\nu_p \approx 0$ for momenta $p$ corresponding to energies equal to the resonant energies. Since by (30) $\kappa_p \approx 1$, we have $g(p) \approx Af(E_p)$. The constant $A$ behaves like $\exp(-\delta V/U_{th})$, i.e. decreases exponentially with increasing applied bias. This can be seen by the expression (31) for $A$: The total number of particles $\mathcal{N}$ will stay constant with increasing bias, whereas the value of $\mathcal{N}_{eq}$ behaves like $\exp(\delta V/U_{th})$. Therefore we get for momenta $p$ with energies close to a resonant energy $g(p) \approx const.\exp(-\delta V)f(E_p)$ and thus $g(p) \approx 0$ for large applied biases. The shape of the I–V characteristic shown in Figure 2 is then explained as follows: For an applied bias smaller than the peak bias of 0.25 V only carriers with energy larger than $-e \max V(x)$, i.e. above the potential bump, and those with energies close to the resonant energy contribute to the current. In the collisional case the distribution function does not weight the states close to the resonant energies as strong as the ballistic distribution function. Therefore the collisional current is smaller than the ballistical current for small biases. For applied biases larger than 0.25 V only the

states with energies above the potential bump contribute to the current. Since—as explained above—the potential bump is lowered by the collisions there are more particles that contribute to the current than in the ballistic case. Thus the collisional current is larger than the ballistically current for large applied biases. This nonphysical blow up of the current density in the collisional case is due to non local effects (in energy) induced by the relaxation time approximation in the Pauli operator $P$: the relaxation time approximation in the operator $P$ allows states to make an energy jump of order $e\delta V$. This energy jump is nonphysical for large applied biases, i.e. large $\delta V$, since in an electron phonon collision event there is only an energy jump of order $\hbar\omega_0$, i.e. of the phonon energy. Mathematically this is expressed by choosing the transition rates $W_{p\to p'}$ of the form $w(p,p')\delta(E_p - E_{p'} \pm \hbar\omega_0)$. The $\delta$–term assures a localization in energy which is missing in the relaxation time approach used here.

Now, we investigate the influence of $\tau$ in the collision case. The interface is again fixed at the $N^+$–$N$ and $N$–$N^+$ junctions and the value of $\tau = \tau_C = \tau_Q$ is changed between $10^{-14}$ s and $10^{-12}$ s. The resulting I–V curve are gathered in Figure 7. We observe that the I–V characteristic is very sensitive with respect to $\tau$. The current peak obtained is larger for larger values of $\tau$. This is due to the increase of collision events and thus an increase of transfer of particles from the left to the right side of the double barrier. Furthermore, we see that for $\tau$ equal to $10^{-12}$ s and $3\cdot 10^{-13}$ s the current peaks are located at a bias of 0.25 V, whereas for $\tau$ larger than $3\cdot 10^{-13}$ s the current peak bias is situated at 0.28 V. For $\tau = 10^{-13}$ s two current peaks are obtained, a flat one at 0.25 V and a peaked one at 0.28 V.

The influence of the interface position was also investigated. The current–voltage characteristics for the ballistic case, if the left interface boundary $x_1$ is moved, are shown in Figure 8. The right interface boundary $x_2$ was fixed at 620 nm and $\tau_C = 3.24\cdot 10^{-13}$s. We see that the left interface boundary cannot be taken to close to the double barrier, since otherwise the quantum resonances are not adequately taken into account. The influence of the right boundary $x_2$ is less strong than that of $x_1$. The I–V curves if the $x_2$ position is changed, are plotted in Figure 9 where $x_1$ is fixed at 500 nm and $\tau_C = 3.24\cdot 10^{-13}$s. We see that $x_2$ can be chosen relatively close to the double barrier, since the high energetic particles in the drain are equally well described by drift–diffusion and quantum models.

The influence of the interface in the collision case is much stronger. The current–voltage characteristics if the position of $x_1$ is changed is plotted in Figure 10. We observe that the current peak is moved to the left, if the $x_1$ position is moved to the right. Also the value of the current peak depends on the position of the $x_1$ interface boundary. The closer $x_1$ is to the double–barrier, the lower the current peak value. The current voltage characteristic, if the $x_2$ position is change is shown in Figure 10. The current peak value is not influenced by the position of $x_2$, but the location of the current peak.

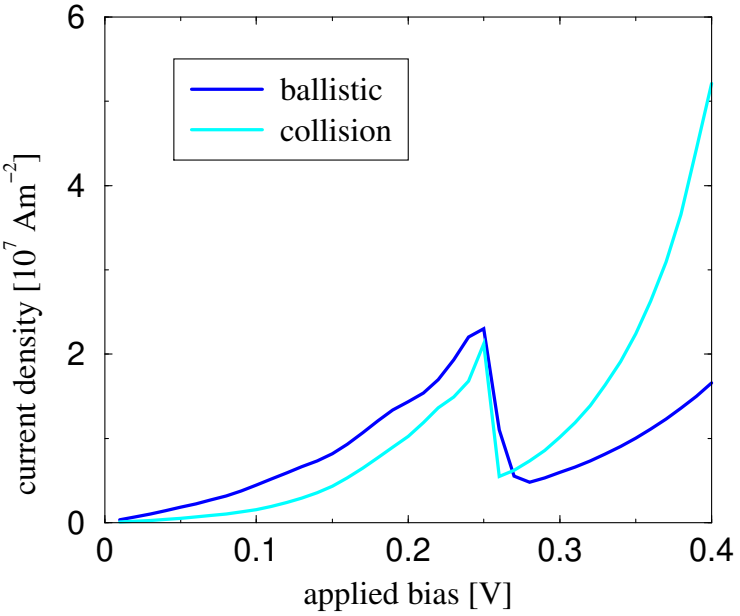


Figure 2: I–V curve in the ballistically and collisional case for the device of Mounaix *et al* [15] where the interface is fixed at $x_1 = 500\,\mathrm{nm}$ and $x_2 = 620\,\mathrm{nm}$ and $\tau_C = \tau_Q = 3.24\,10^{-13}\,\mathrm{s}$.

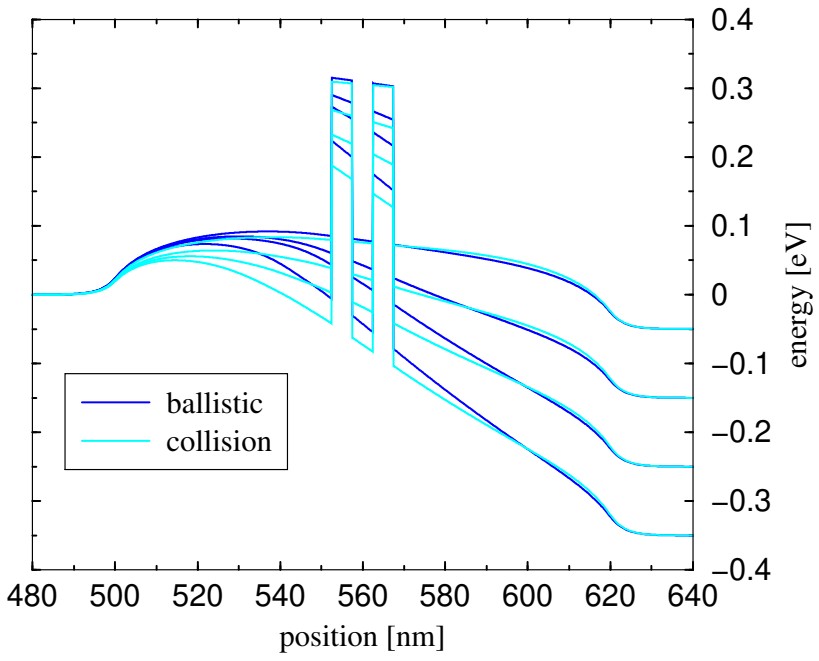


Figure 3: Potential profile in the ballistically and collisional case for the device of Mounaix et al [15] where the interface is fixed at $x_1 = 500\,\mathrm{nm}$ and $x_2 = 620\,\mathrm{nm}$ and $\tau_C = \tau_Q = 3.24\,10^{-13}\,\mathrm{s}$.

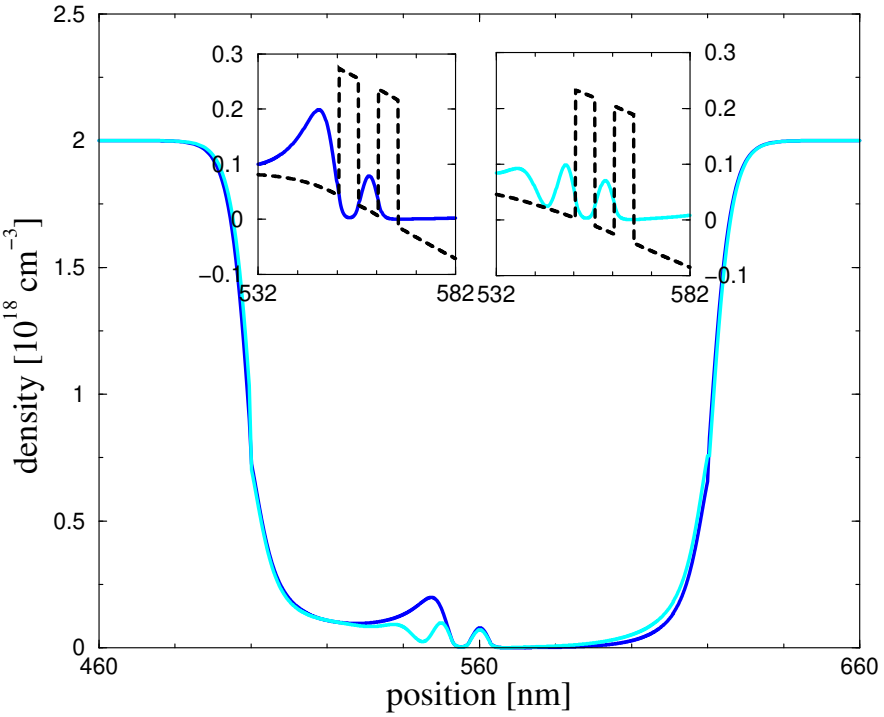


Figure 4: Density profile at the current peak bias 0.25 V in the ballistically case (blue) and collisional case (cyan).

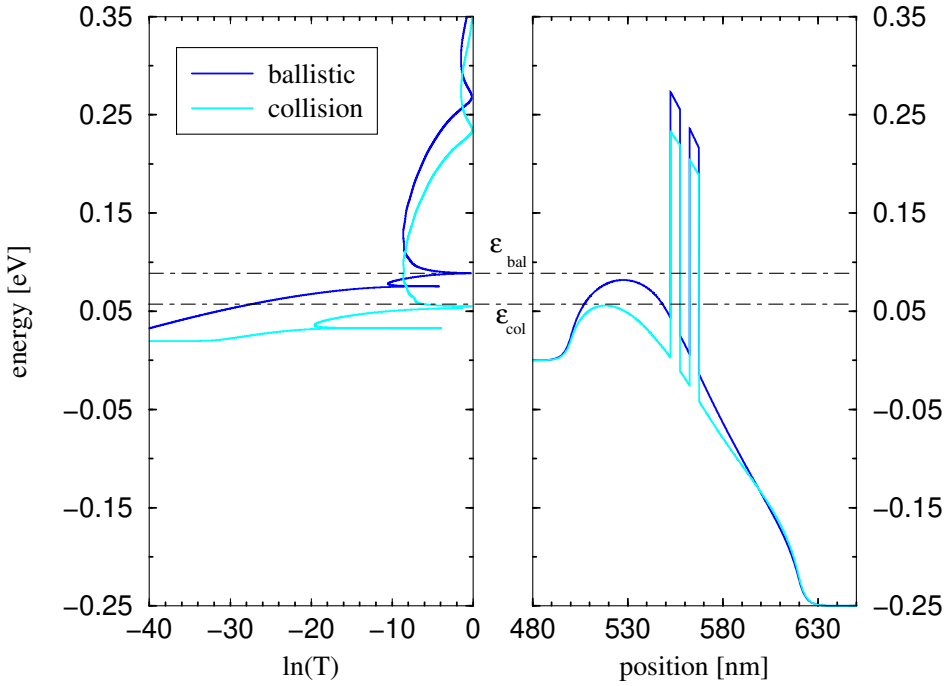


Figure 5: Transmission coefficient and potential profile for the current peak bias 0.25 V. $\epsilon_{bal}$, $\epsilon_{col}$ denote the resonance energy in the ballistically and collisional case, respectively.

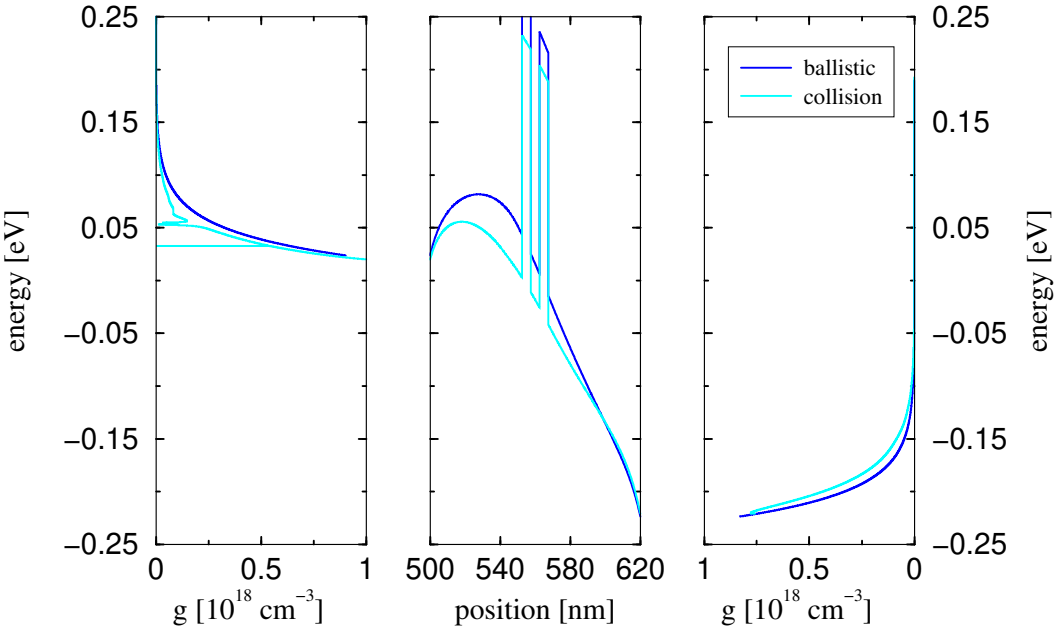


Figure 6: Distribution function $g$ and potential profile for the current peak bias 0.25 V.

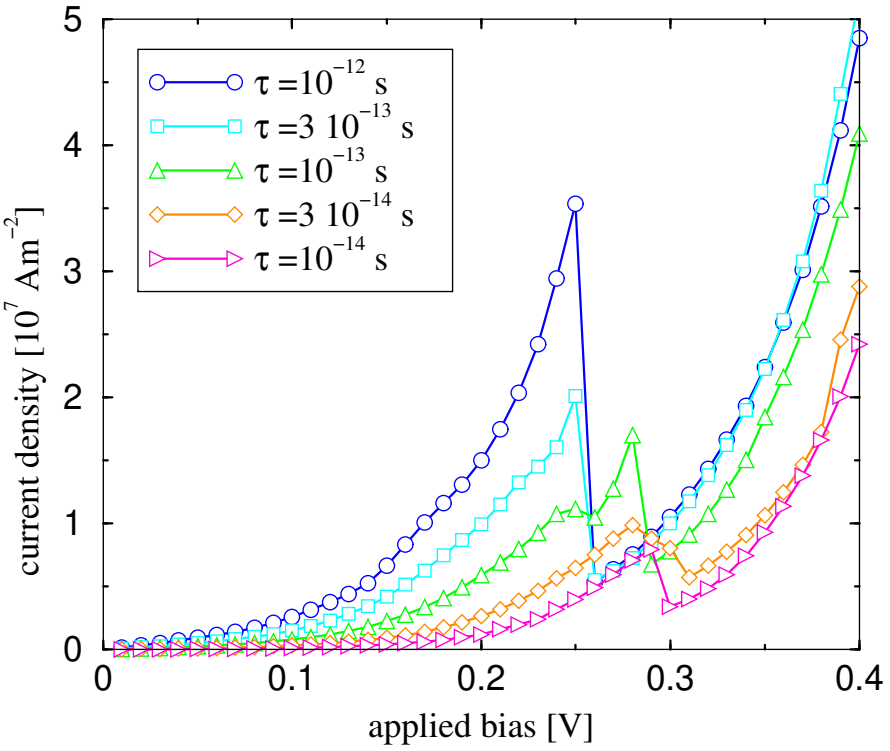


Figure 7: I–V characteristics of the device [15] for different values of $\tau$.

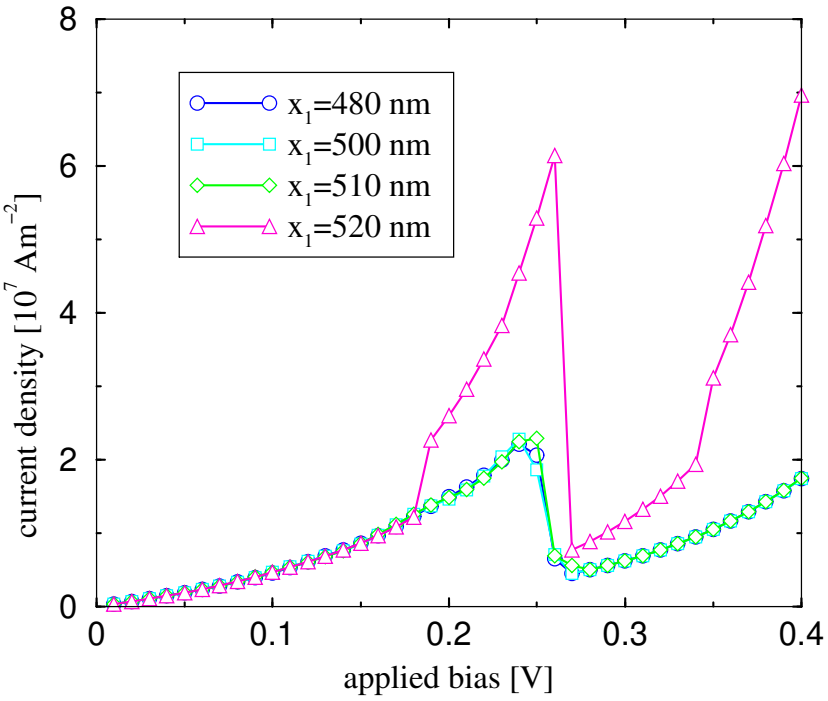


Figure 8: I–V curve in the ballistic case if the interface boundary $x_1$ is moved and $x_2$ is fixed at 620 nm.

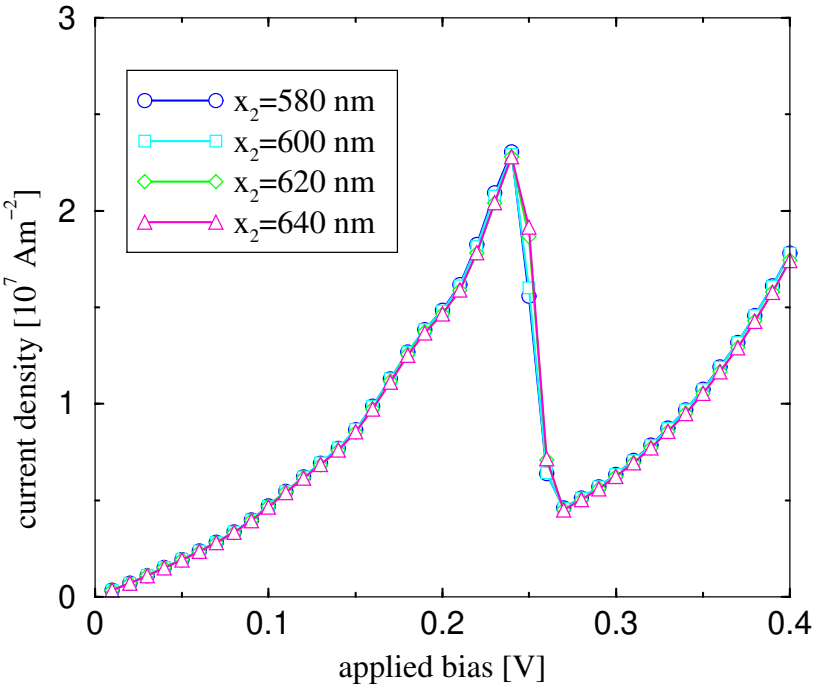


Figure 9: I–V curve in the ballistically case if the interface boundary $x_2$ is moved and $x_1$ is fixed at 500 nm.

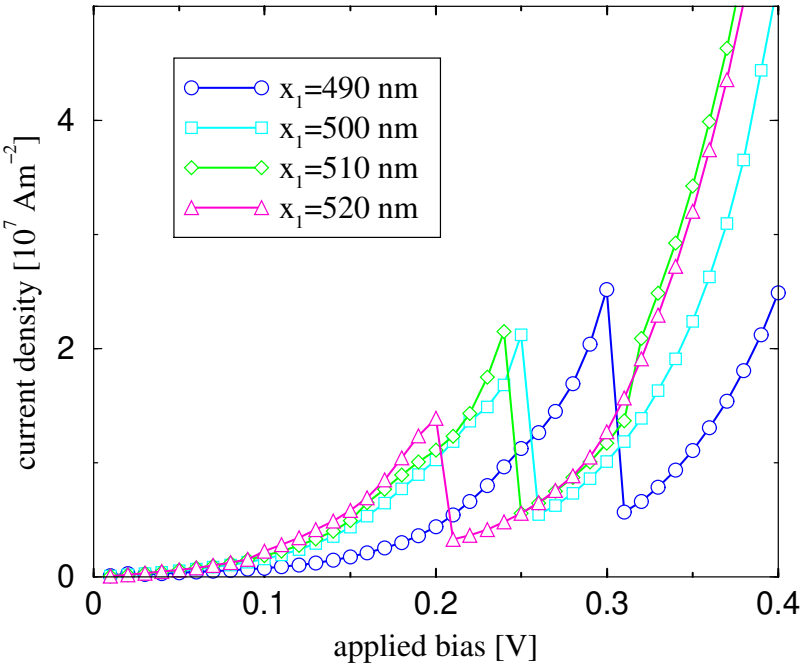


Figure 10: I–V curve in the collisional case if the interface boundary $x_1$ is moved. $x_2$ is fixed at 620 nm and $\tau = \tau_C = \tau_Q = 3.24\,10^{-13}$ s.

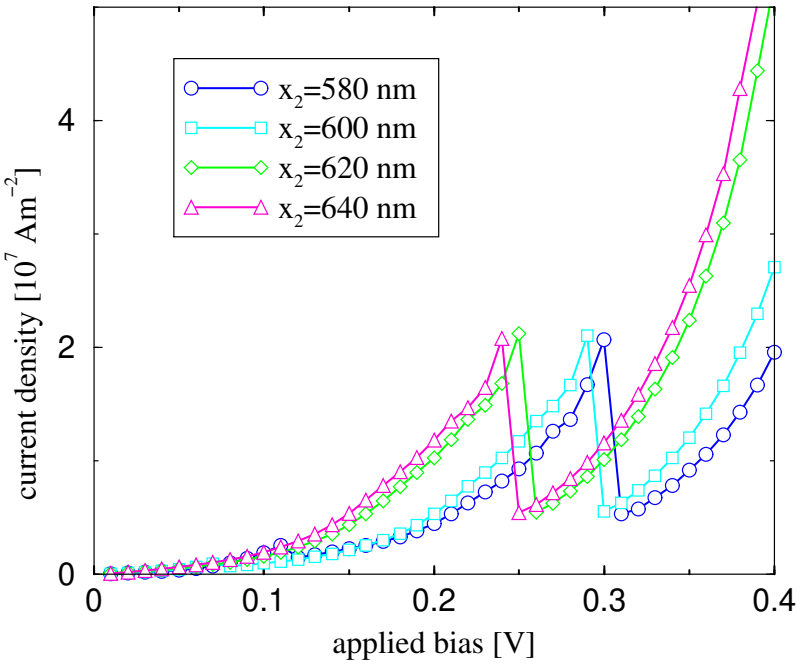


Figure 11: I–V curve in the collisional case if the interface boundary $x_2$ is moved. $x_1$ is fixed at 500 nm and $\tau = \tau_C = \tau_Q = 3.24 \cdot 10^{-13}$ s.

### 3.2 The RTD of Kluksdahl *et al* [14]

In this subsection we consider the resonant tunneling device geometry of [14]. The schematic geometry of this device is shown in Figure 12 and the physical parameters are summarized in Table II, where $\tau = \tau_C = \tau_Q$ and $H$ is the hight of the double barrier.

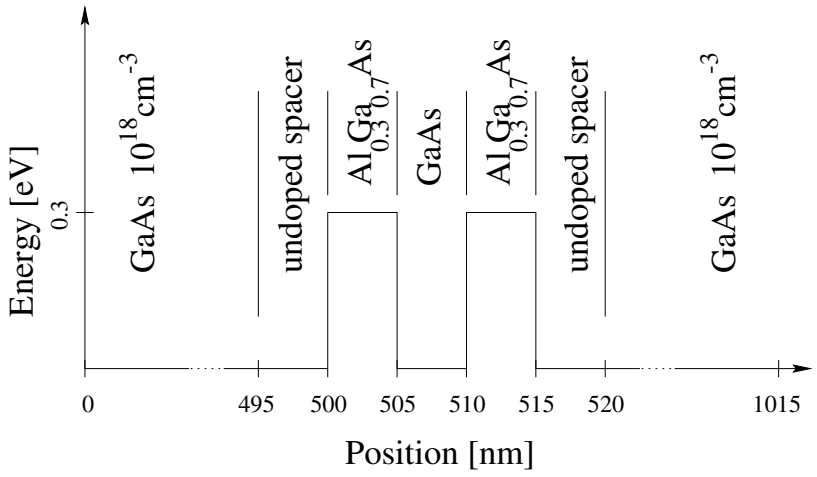


Figure 12: The double barrier resonant tunneling structure of [14]

| $m$ | $\epsilon_1$ | $\epsilon_2$ | $\tau$ [s] | $T$ [K] | $H$ [eV] |
|---|---|---|---|---|---|
| $0.069m_0$ | $13.1\epsilon_0$ | $12.3\epsilon_0$ | $1.17\,10^{-13}$ | 300 | 0.3 |

Table II: Physical parameters for the device of [14], where the index 1 refers to the GaAs regions and 2 to the barrier region

The calculated I–V curve is plotted in Figure 13 for the ballistic and collision case, where the interface boundaries are fixed at $x_1 = 490\,\text{nm}$ and $x_2 = 530\,\text{nm}$. As for the previous device, we observe that the current peak of the current–voltage characteristics is lower for the collision current. The current peak is located for both cases at an applied bias of 0.26 V. The blow up of the collision current for high applied biases is again due to the non local effects of the relaxation time approximation in the collision operator of the Pauli master equation. The potential profiles for the current peak bias is shown in Figure 14. The results obtained here in the ballistic case compare well with those of [6] and those of [14], where a Wigner formulation was used for the calculations.

The density profile for the current peak bias is shown in Figure 15. Note the large discontinuity of the density in the collision case. The quantum density calculated at the interface boundary $x_1$ is lower compared to the classical density at $x_1$. The contrary is true at the $x_2$ boundary, i.e. the quantum density is larger than the classical density at $x_2$. This reflects the transport of particles from the left to the ride side of the double barrier due to collisions.

The influence of the interface position has also been investigated. The current–voltage characteristics, if the $x_1$ position is moved, is shown in Figure 16 in the ballistic and in Figure 17 in collision case. As in [6] we see that for $x_1 = 470\,\text{nm}$ the ballistic I–V characteristic has a monotone behavior. In [6] it was presumed that this was due to the neglection of collisions in the quantum zone, because a negelection of collisions in large regions is known to lead to non physical current–voltage characteristics. In fact Figure 17, where collisions in the quantum region are included, shows that for $x_1 = 470\,\text{nm}$ the I–V characteristic is in fact non monotone as it should be. As in the previous device the high current for large applied biases is again due to the non local effects in energy space described before.

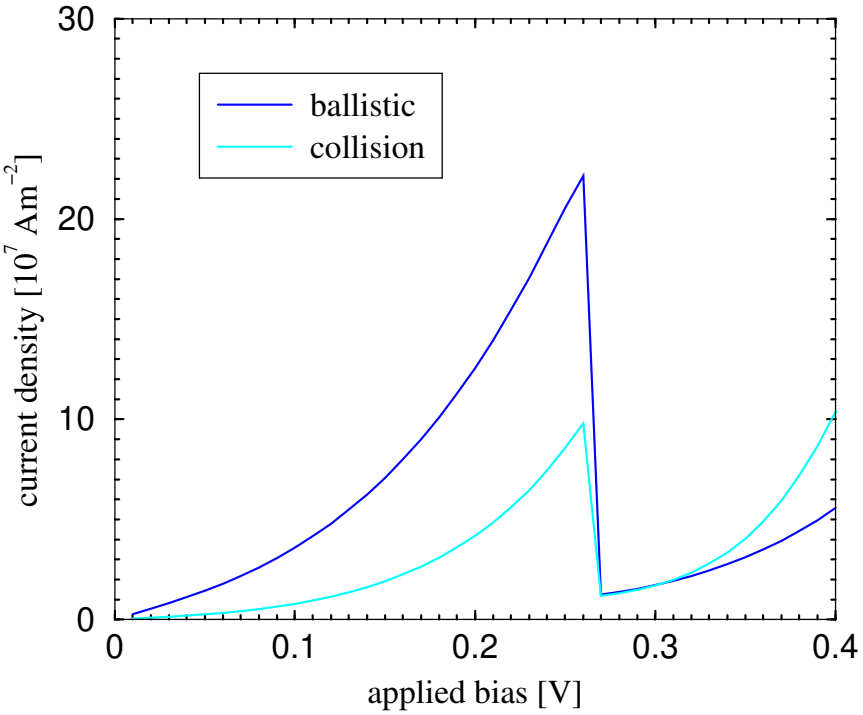


Figure 13: I–V curve of the device [14] where $x_1 = 490\,\text{nm}$ and $x_2 = 530\,\text{nm}$.

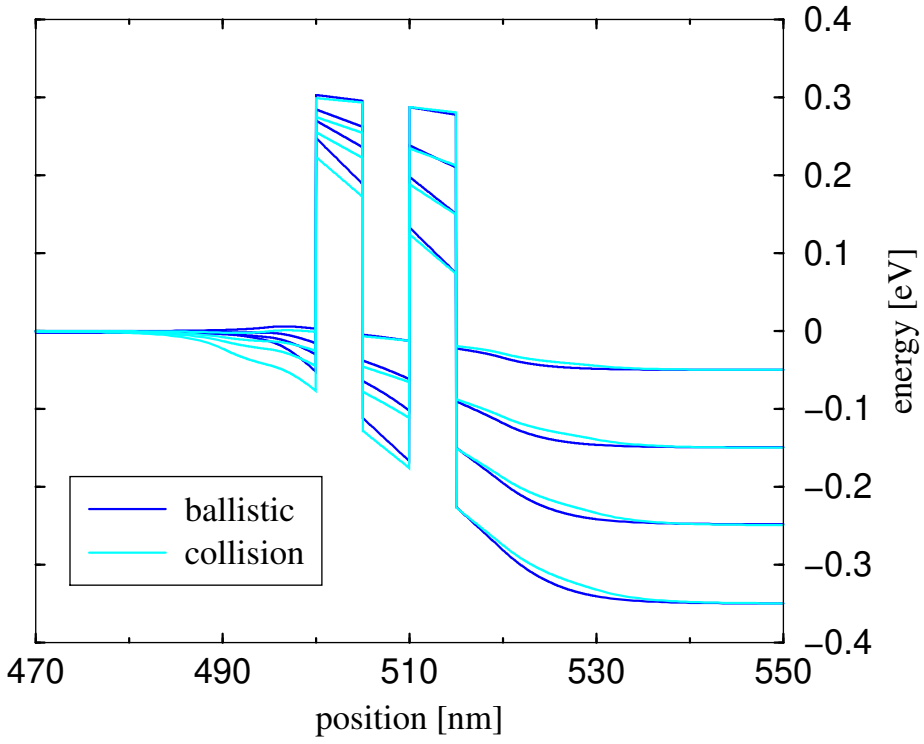


Figure 14: Potential profiles for the device of [14].

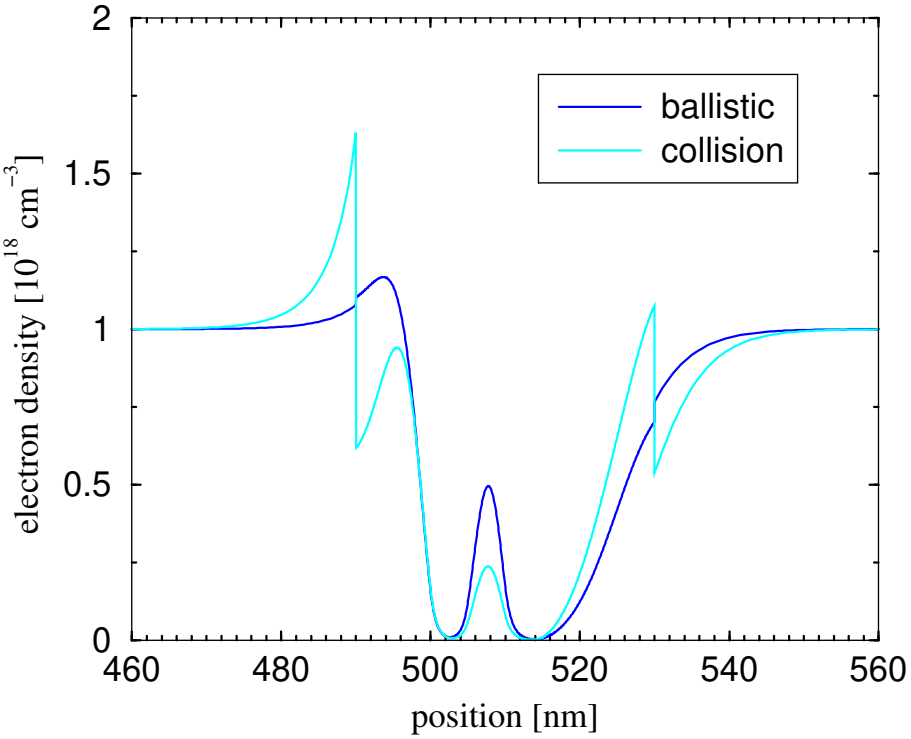


Figure 15: Density profile for the current peak bias 0.26 V for the device of [14].

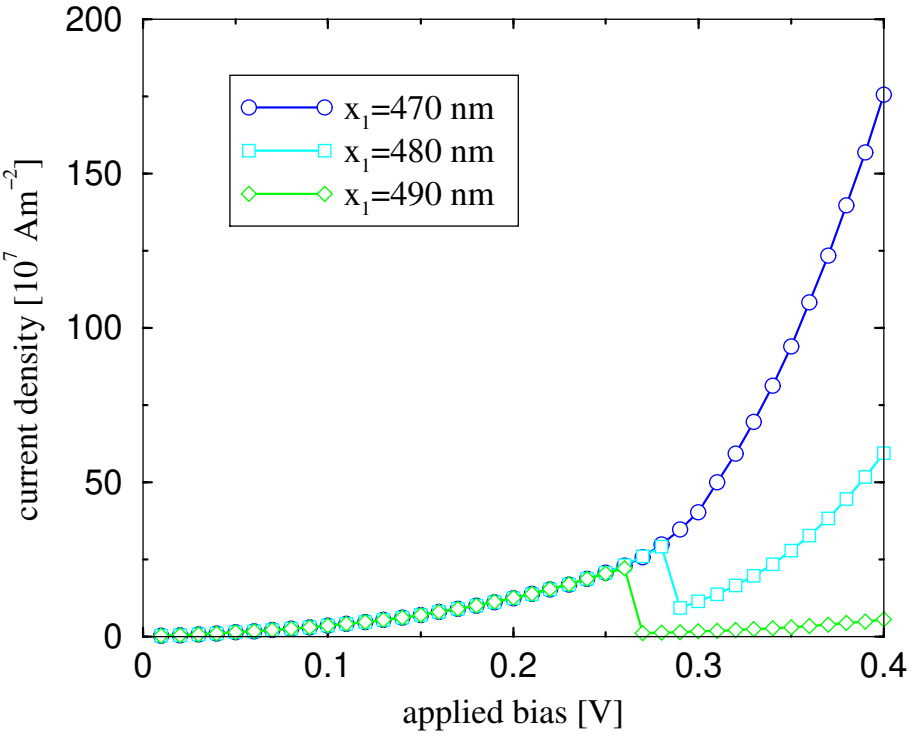


Figure 16: I–V characteristic when the interface $x_1$ is moved in the ballistically case.

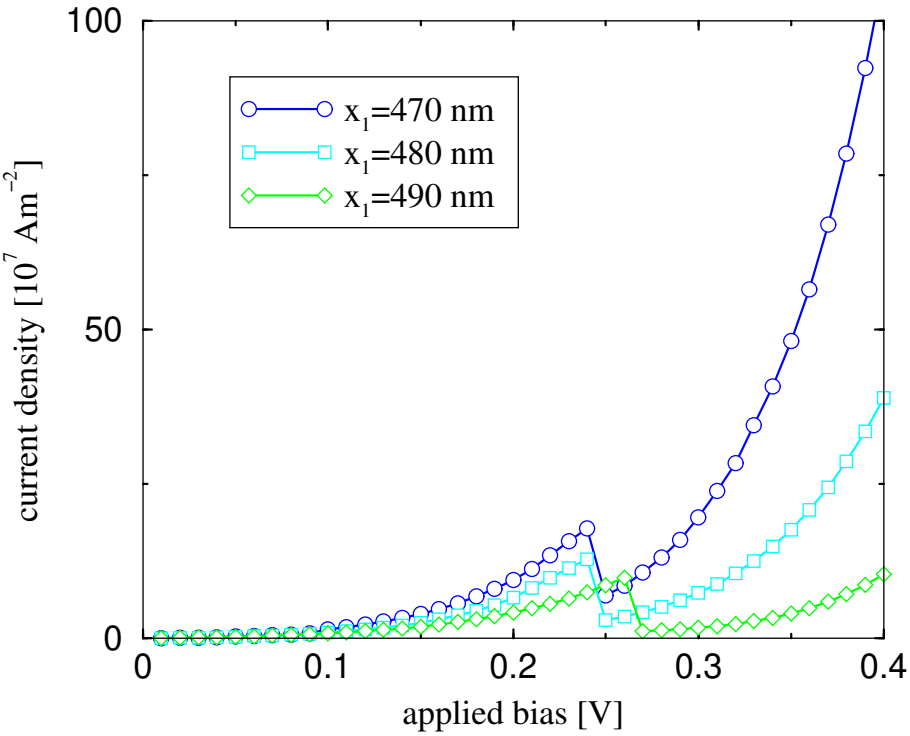


Figure 17: I–V characteristic when the interface $x_1$ is moved in the collisional case.

### 3.3 The RTD of Fischetti [8]

The last device we consider in this paper is that of Fischetti [8]. Compared to the previous devices the size of this resonant tunneling diode is much smaller (316.1 nm). The geometry of the device is shown in Figure 18 and the physical parameters used for the calculation are gathered in Table III. For the collisional calculations we se $\tau_Q = \tau_C = \tau$. The calculated I–V curve for the interface position $x_1 = 147$ nm and $x_2 = 171.1$ nm are plotted in Figure 19 for the ballistically and collisional simulations. The current peak in the ballistically case is observed at an applied bias of 0.37 V and the peak value is $92 \cdot 10^7$ Am$^{-2}$. In [8] the current peak is obtained at an applied bias of 0.4 V with a value of $130 \cdot 10^7$ Am$^{-2}$. The model used in [8] for the ballistic simulations is completely ballistic whereas our model is only ballistic in the quantum region. This explains the fact that our obtained current peak value is larger than that obtained by Fischetti.

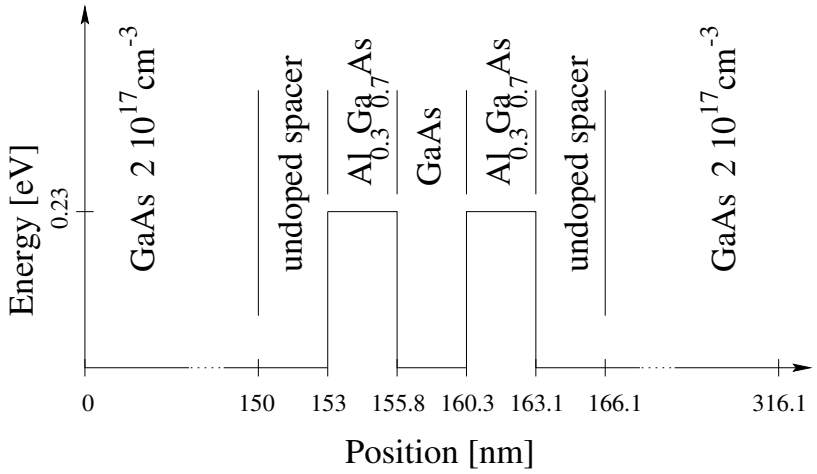


Figure 18: The double barrier resonant tunneling structure of [8]

| $m_1$ | $m_2$ | $\epsilon_1$ | $\epsilon_2$ | $\tau$ [s] | $T$ [K] | $H$ [eV] |
|---|---|---|---|---|---|---|
| $0.067m_0$ | $0.149m_0$ | $12.09\epsilon_0$ | $10.92\epsilon_0$ | $3.24\ 10^{-13}$ | 300 | 0.23 |

Table III: Physical parameters for the device of [8], where the index 1 refers to the GaAs regions and 2 to the barrier region

In the collisional case we observe one current peak at an applied bias of 0.35 V with a value of $62 \cdot 10^7$ Am$^{-2}$, see Figure 19. The I–V curve of Fischetti two current peaks are observed. A flat one at an applied bias of 0.2 V with $70 \cdot 10^7$ Am$^{-2}$ and a peaked one at 0.43 V with a current density of $220 \cdot 10^7$ Am$^{-2}$. The different shape of the I–V curves observed here is explained by the different Pauli operator used in [8]: In [8] a more complex Pauli operator $P$ is used which takes into account nonpolar scattering with acoustic phonons, polar and nonpolar scattering with optical phonons. Here we used a relaxation time approximation for the operator $P$ in the master equation. Furthermore, we note that in [8] convergence problems appeared in the self–consistent computation of the electrostatic potential in the collisional case around the current peaks. In our simulations we did not observe any convergence problems. For large applied biases we do not observe a blow up of the current density in the collisional simulations which appeared in the I–V characteristics of the devices discussed before. This is due to the small size of the quantum zone such that the non–local effects leading to the blow up is not as strong as for the other devices. This is also reflected in the potential profile plotted in Figure 20 and the density profile shown in Figure 21. The resulting I–V curves if the left interface boundary is moved ($x_2$ is fixed

at 172.1 nm) are shown in Figure 22 and 23 for the ballistically and collisional case, respectively. We observe—as in the device of Kluksdahl *et al* [14]—that the best results are obtained if left interface is chosen close to the double barrier.

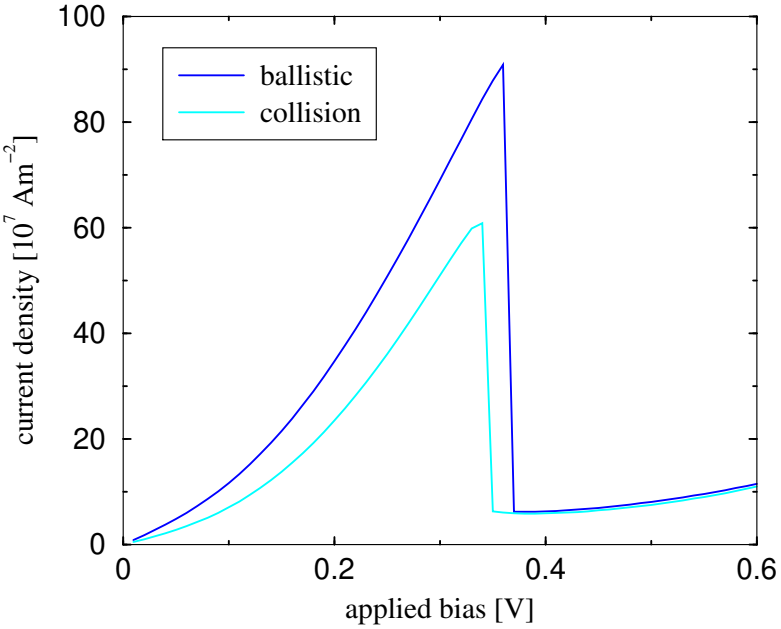


Figure 19: I–V curve of the device [8] where $x_1 = 147\,\text{nm}$ and $x_2 = 171.1\,\text{nm}$.

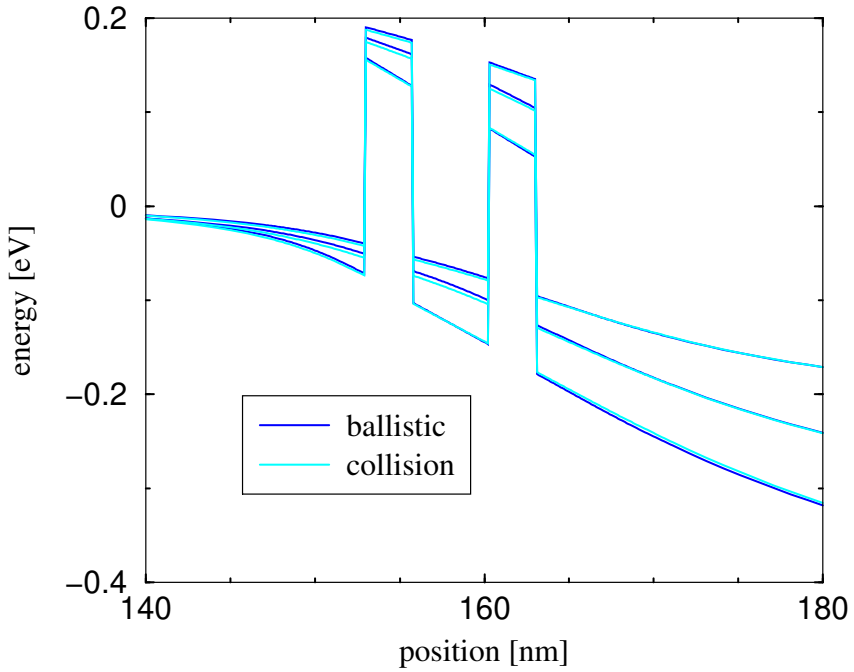


Figure 20: Potential profile for applied biases of 0.2 V, 0.3 V and 0.4 V of the device [8]. The quantum interface is chosen at $x_1 = 147$ nm and $x_2 = 171.1$ nm.

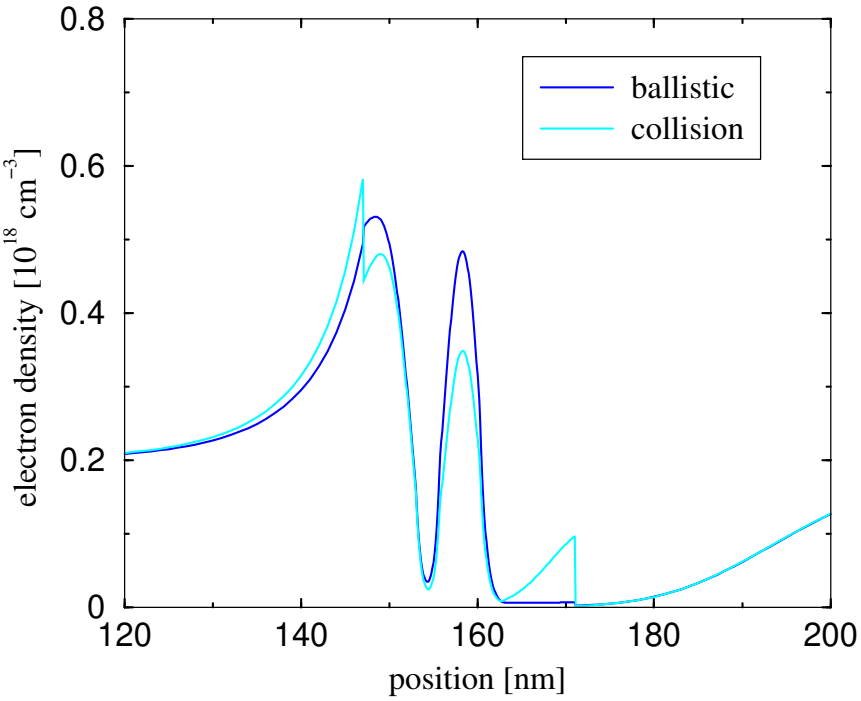


Figure 21: Density profile for an applied bias of 0.36 V of the device [8].

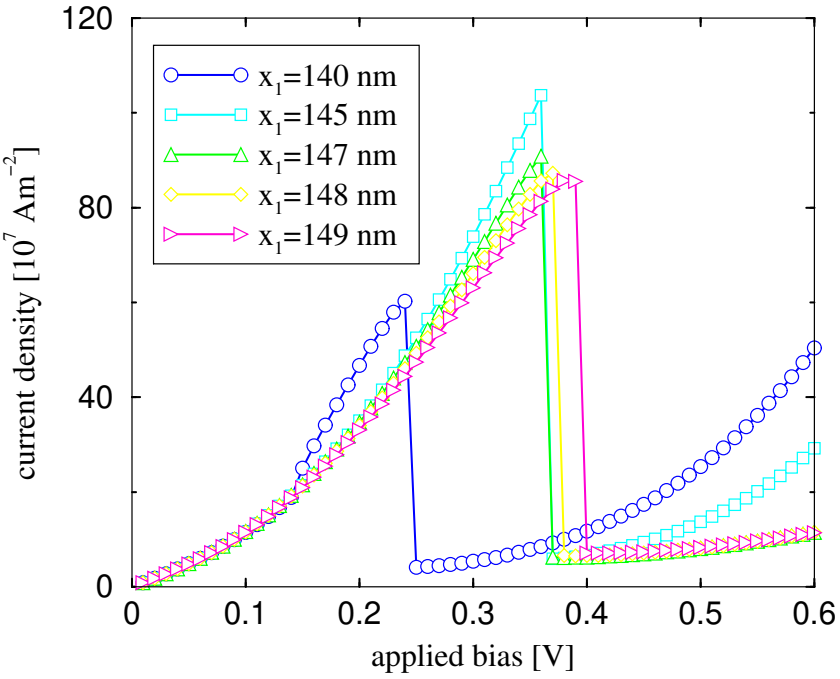


Figure 22: I–V characteristic for the device of [8] when the interface $x_1$ is moved in the ballistically case. The position of $x_2$ is fixed at 171.1 nm.

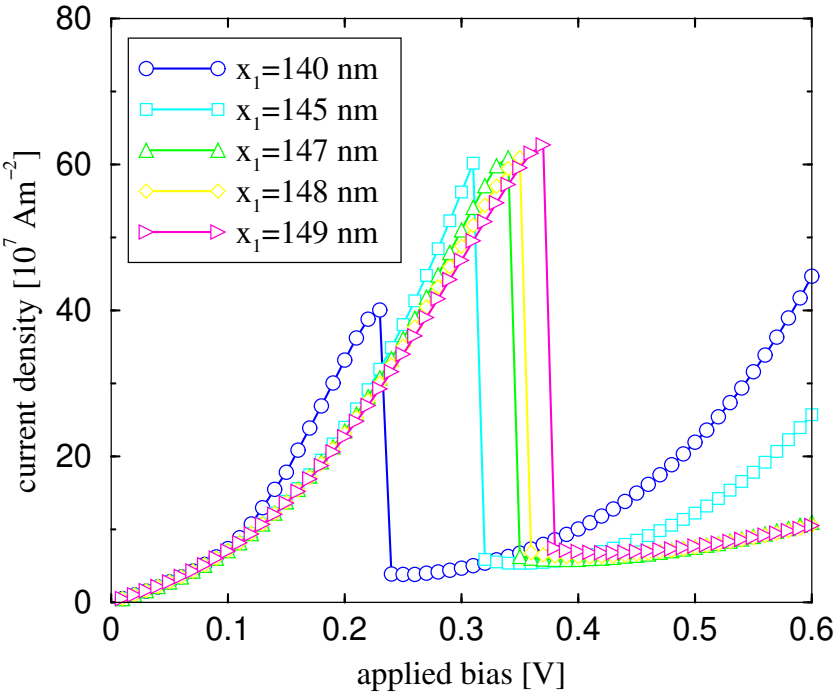


Figure 23: I–V characteristic for the device of [8] when the interface $x_1$ is moved in the collisional case. The position of $x_2$ is fixed at 171.1 nm.

# 4 Summary and Conclusion

We presented a method to couple drift–diffusion and quantum models in a one dimensional stationary framework. Collisions in the quantum region have been introduced by a Pauli master equation, which consists of a collision operator $P$ (Pauli operator) and an operator $C$ which takes into account the interaction with the classical regions. A relaxation time approximation was used for the operator $P$ which allows an explicit expressions of the distribution function $g$, see (29). The two models are coupled such that a continuity of the current density is guaranteed. This was achieved by introducing the coupling constant $\Theta$. The coupling strategy presented in this paper was compared to that used in [6] in the ballistically case. In contrast to [6] we found an analytic expression for the coupling constant $\Theta$, see (24), and guarantee a continuity of the current density over the whole device domain. The model has been numerically implemented and validated against three resonant tunneling diode test cases. If the quantum zone is chosen properly, good numerical results are obtained in the ballistically case. The relaxation time approach gives good results for small applied biases, but a non physical blow up of the current was observed for large applied biases. This effect is due to a non local effect in energy space due to the relaxation time approximation. This should be cured by using a more realistic electron phonon collision operator $P$. Especially the $\delta$–terms should prevent this non local effects. The influence of the position of the quantum region has been investigated. Furthermore we showed that the results are very sensitive with respect to the relaxation time $\tau$.

# Acknowledgements

Part of this work was carried out while M.B. was visiting the institute Mathématiques pour l'Industrie et la Physique (MIP), Toulouse, in the framework of a fellowship of the EU research training network

HYKE, EU contract no. HPRN-CT-2002-00282, and he would like to thank P. Degond, N. Ben Abdallah and the MIP for their hospitality. M.B. is supported by the DFG Research Center "Mathematics for key technologies" (FZT 86) in Berlin. The financial support of the bilateral cooperation program Procope D/0205756 funded by the DAAD is also gratefully acknowledged.

# References

[1] M. Baro, H.-Chr. Kaiser, H. Neidhardt, J. Rehberg, *A quantum transmitting Schrödinger-Poisson system*, WIAS-Preprint **814**, Weierstrass Institute for Applied Analysis and Stochastics (to appear in Rev. Math. Phys.), 2003.

[2] M. Baro, *Analysis of a coupled Schrödinger drift–diffusion model*, (in preparation).

[3] N. Ben Abdallah, *A hybrid kinetic-quantum model for stationary electron transport in a resonant tunneling diode*, J. Stat. Phys. **90**:627–662, 1998.

[4] N. Ben Abdallah, P. Degond, P.A. Markowich, *On a one-dimensional Schrödinger–Poisson scattering model*, ZAMP **48**:135–155, 1997.

[5] V. Buslaev, V. Fomin, *An inverse scattering problem for the one dimensional Schrödinger equation on the entire axis*, Vestnik Leningrad Univ. **17**:56–64, 1962.

[6] P. Degond, A. El Ayyadi, *A coupled Schrödinger drift–diffusion model for quantum semiconductor device simulations*, J. Comp. Phys. **181**:222–259, 2002.

[7] A. El Ayyadi, *Couplage des Modèles Classique-Quantique Simulation de la Diode À Effet Tunnel*, Ph.D. thesis, Institute National des Sciences Appliquées de Toulouse, 2002.

[8] M.V. Fischetti, *Theory of electron transport in small semiconductor devices using the Pauli master equation*, J. Appl. Phys. **83** (1):270–291, 1998.

[9] M.V. Fischetti, *Master-equation approach to the study of electronic transport in small semiconductor devices*, Phys. Rev. B **59**(7):4901–4917, 1999.

[10] W.R. Frensley, *Quantum transport*, In: N.G. Einspruch, W.R. Frensley (eds.), *Heterostructures and Quantum Devices*, Academic Press, New York, 1994.

[11] W.R. Frensley, *Boundary conditions for open quantum systems driven far from equilibrium*, Reviews of Modern Physics **62**:745–791, 1990.

[12] H. Gajewski, K. Gröger, K. Zacharias, *Nichtlineare Operatorgleichungen und Operatordifferentialgleichungen*, Akademie Verlag, Berlin, 1974.

[13] H. Gajewski, *Analysis und Numerik von Ladungstransport in Halbleitern*, Mitt. Ges. Angew. Math. Mec. **16**: 35–57, 1993.

[14] N.C. Kluksdahl, A.M. Kriman, D.K. Ferry, C. Ringhofer, *Self-consistent study of the resonant-tunneling diode*, Phys. Rev. B **39** (11):7720–7735, 1989.

[15] P. Mounaix, O. Vanbesien, D. Lippens, *Effect of cathode spacer layer on the current-voltage characteristics of resonant tunneling diodes*, Appl. Phys. Lett. **57** (15):1517–1519, 1990.

[16] W. Pauli, *Festschrift zum 60. Geburtstage von A. Sommerfeld*, Hirzel, Leipzig, p. 30, 1928.

[17] W. van Roosbroeck, *Theory of flow of electrons and holes in germanium and other semiconductors*, Bell Syst. Techn. J. **29**:560–607, 1950.

[18] S. Selberherr, *Analysis and Simulation of Semiconductor Devices*, Springer-Verlag Wien, 1984.

[19] R. Tsu, L. Esaki, *Tunneling in a finite superlatice*, Appl. Phys. Lett. **22**(11):562–564, 1973.

# List of Figures


1 The double barrier resonant tunneling structure of [15] . . . 11
2 I–V curve in the ballistically and collisional case of the device [15] . . . 13
3 Potential profiles for the device of [15] . . . 13
4 Density profile of the device of [15] . . . 14
5 Transmission coefficient and potential profile of the device of [15] . . . 14
6 Distribution function and potential profile for the device of [15] . . . 15
7 I–V characteristics of the device [15] for different values of $\tau$. . . . 15
8 Ballistically I–V curve of the device of [15] for different $x_1$. . . . 16
9 Ballistically I–V curve of the device of [15] for different $x_2$. . . . 16
10 Collisional I–V curve of the device of [15] for different $x_1$. . . . 17
11 Collisional I–V curve of the device of [15] for different $x_2$. . . . 17
12 The double barrier resonant tunneling structure of [14] . . . 18
13 I–V curve in the ballistically and collisional case of the device [14] . . . 19
14 Potential profiles for the device of [14]. . . . 19
15 Density profile of the device of [14]. . . . 20
16 Ballistically I–V curve of the device of [14] for different $x_1$. . . . 20
17 Collisional I–V curve of the device of [14] for different $x_1$. . . . 21
18 The double barrier resonant tunneling structure of [8] . . . 22
19 I–V curve in the ballistically and collisional case of the device [8]. . . . 23
20 Potential profiles for the device of [8]. . . . 23
21 Density profile of the device of [8]. . . . 24
22 Ballistically I–V curve of the device of [8] for different $x_1$. . . . 24
23 Collisional I–V curve ofthe device of [8] for different $x_1$. . . . 25


# List of Tables


I Physical parameters for the device of [15]. . . . 10
II Physical parameters for the device of [14]. . . . 18
III Physical parameters for the device of [8]. . . . 22